Dermal Fibroblast Infiltration of Poly(ε-caprolactone) Scaffolds Fabricated by Melt Electrospinning in a Direct Writing Mode

Brooke L Farrugia[1*], Toby D Brown[2], Zee Upton[1], Dietmar W. Hutmacher[2], Paul D Dalton[2] and Tim R. Dargaville[1]

Affiliations

1. Tissue Repair and Regeneration Program, Institute of Health and Biomedical Innovation, Queensland University of Technology, Brisbane, Australia

2. Regenerative Medicine Program, Institute of Health and Biomedical Innovation, Queensland University of Technology, Brisbane, Australia

* = corresponding author, brooke.farrugia@qut.edu.au

Short title: Fibroblast Infiltration of Scaffolds Fabricated by Melt Electrospinning in a Direct Writing Mode

Abstract

Melt electrospinning in a direct writing mode is a recent additive manufacturing approach to fabricate porous scaffolds for tissue engineering applications. In this study we describe porous andcell-invasive poly (ε-caprolactone) scaffolds fabricated by combining melt electrospinning and a programmable x-y stage. Fibers were 7.5 ± 1.6 μm in diameter and separated by interfiber distances ranging from 8 μm to 133 μm, with an average of 46 ± 22 μm. Micro-computed tomography revealed the resulting scaffolds had a highly porous (87%), three-dimensional structure. Due to the high porosity and interconnectivity of the scaffolds, a top-seeding method was adequate to achieve fibroblast penetration, with cells present throughout and underneath the scaffold. This was confirmed histologically, whereby a 3D fibroblast-scaffold construct with full cellular penetration was produced after 14 days *in vitro*. Immunohistochemistry was used to confirm the presence and even distribution of the key dermal extracellular matrix proteins, collagen type I and fibronectin. These results show that melt electrospinning in a direct writing mode can produce cell invasive scaffolds, using simple top-seeding approaches.

1. Introduction

Interest in scaffolds for tissue engineering (TE) applications fabricated using additive manufacturing (AM) principles is continually increasing as crucial parameters can be systematically controlled. Scaffold thickness, filament diameter, pore size and interconnectivity required for cell invasiveness can all be altered in a broad range of morphologies [1-5]. One melt extrusion based AM approach, namely fuse deposition modeling (FDM), permits the accurate control of scaffolds properties; however, the lower limit of filament diameter is restricted to approximately 100 μm due to the viscosity of the polymer melt being extruded through a small diameter orifice [1, 6]. Significantly lower filament resolutions can be achieved in a separate AM process using colloidal ink systems deposited in a direct writing mode [1, 2, 7, 8]. This approach uses colloidal systems to produce orderly substrates with fiber diameters between approximately 0.5 μm and 10 μm [1]. However, biomaterials need to be formulated into polyelectrolyte inks and significant manufacturing times are needed to manufacture the scaffolds [6].

The orderly structures of such AM produced scaffolds contrast with the non-woven nanofibrous meshes produced by electrostatic drawing (electrospinning) [9]. Electrospun meshes demonstrate excellent *in vitro* compatibility, however, most meshes perform as substrates [10-13], rather than scaffolds that permit cell infiltration, as they have pores sizes too small to allow cell invasion [6, 14-16]. While there are reports of penetration into electrospun meshes, these are typically restricted to depths of less than 150 μm and complex and taxing strategies are needed to create open pores [17-19].

This importance of cell invasiveness has been recognized by many electrospinning researchers and has prompted investigation of approaches to produce cell-invasive scaffolds [20]. These include electrospinning onto ice crystals as they grow off a collector [21, 22], salt leaching [23], retrieving fibers collected onto water (hydrospinning) [24], and electrospinning onto patterned [25-27] and complex collectors through the use of needle-like probes attached to a flat collecting surface [28]. In addition, bimodal scaffolds have been recently described in which solution electrospinning is combined with larger scale fabrication techniques to increase the pore size [20, 29-

33]. This emerging trend of bimodal scaffolds provides a straightforward approach to produce cell invasive scaffolds while utilizing the benefits of sub-micron filaments. In another study, solution electrospinning was combined with melt electrospinning, to create a bimodal scaffold where the larger melt electrospun fibers combined with smaller solution electrospun fibers resulted in a 3D cell-invasive scaffold [30]. Melt electrospun meshes typically have diameters between 2 and 20 μm [9, 34, 35].

In addition to slightly larger fibers, the non-conductive and viscous electrified jet produced during melt electrospinning can be accurately deposited [36] making it suitable as a direct-writing technique to produce scaffolds with accurately placed fibers stacked on top of each other [37, 38]. This process allows for scaffold pore size to be tailored, paving the way for better control over cell invasiveness. Melt electrospinning in a direct writing mode is therefore a new AM approach to produce orderly scaffolds for TE applications.

One area that can benefit from this new fabrication technique is the development of dermal substitutes. Early examples of dermal substitutes for formation of an *in vitro* skin equivalent have been reported using collagen gels [39-41]. Bell *et al.* [40, 41] were able to demonstrate a collagen based dermal substitutes supported keratinocyte differentiation, however, a fundamental limitation associated with the use of collagen is contraction of the gels [42]. This limitation has not gone unnoticed, with many studies carried out in an attempt to find alternative constructs [43-46]. One study conducted by Ng *et al.* [47] compared two commercially available collagen based matrices with two non-collagen based scaffolds, fabricated from both natural and synthetic polymers. While it was shown that three out of the four scaffold types were capable of supporting the formation of dermal-like tissue, it was noted that for the non-collagen based scaffold that supported tissue formation, the dermal fibroblasts were unable to completely infiltrate the scaffold structure, highlighting the importance of scaffolds that allow cell infiltration.

This paper details melt electrospinning in a direct writing mode to produce scaffolds, which are cell invasive *in vitro*. We investigated the scaffold morphology with scanning electron microscopy (SEM) and micro-computed tomography (μ-CT), showing that the scaffolds' pores are both

interconnected and cell invasive, with excellent fibroblast infiltration after a simple top-seeding method and culturing under static conditions. Furthermore, we demonstrate that important dermal extracellular matrix (ECM) proteins are produced within the cell-scaffold construct via immunohistochemical methods.

2. Experimental Methods

2.1. Scaffold Fabrication

Melt electrospun scaffolds were fabricated based on a direct writing approach previously described, where a translating x-y stage is used to collect the fibers [37]. Briefly, poly(ε-caprolactone) (PCL) (Perstorp, M_n ~ 83 kDa), pellets were placed into a 2 mL luer lock syringe (B-Braun, Australia) and heated to 80 °C in an oven overnight to remove any air bubbles from the melt. A blunt 23 G needle acting as the spinneret was attached to the syringe and placed into a water circulating system heated to 78 °C. The PCL melt was then electrospun using a collector distance of 30 mm, a flow rate of 10 μL/h and a voltage of 10 kV applied to the spinneret. Writing with the PCL fibers was achieved by collecting on a grounded plate connected to a programmable x-y stage, controlled using Mach 3 software. A schematic of the electrospinning writing apparatus is shown in figure 1(a). The programmed design (figure 1(b)) consisted of interlaced diagonal lines at a translational velocity of 2.5×10^{-2} m/s, which was looped four times for each scaffold. Scaffolds with randomly deposited fibers were prepared on an alternative in-house built apparatus with a static collection stage [48], under comparable conditions.

2.2. Scaffold Characterization

Scaffolds were visualized using light microscopy (Zeiss, Axio Scope) prior to seeding cells. Images were recorded using Axio Vision software (version 4.8.2) at three positions along the z-axis and were then analyzed using Image J (Version 1.45c, NIH) to determine both fiber diameter and interfiber distance (10 measurements per image). From this, each scaffold was directly assessed in terms of fiber diameter and distance between fibers prior to *in vitro* experiments. An overall

assessment of the scaffold was achieved using μ-CT (Xradia MicroXCT-400) where a representative sample was scanned at a resolution of 0.786 μm, 80 kV, and an integration time of 50 s. Scaffold porosity was obtained by applying a bone morphometric analysis algorithm that determines the ratio of volume occupied by the scaffold fibers to the total volume scanned [49]. Optical images of the scaffold were taken on a Canon power shot A620 digital camera attached to a stereomicroscope (Stemi 2000C, Zeiss) fitted with a digital camera adapter (426126, Zeiss).

2.3. Dermal Fibroblast Isolation

Primary human dermal fibroblasts were isolated from surgical discards of consenting patients undergoing elective surgery. Ethics approval was obtained from the Queensland University of Technology's Review Board (3673H) and associated hospitals, along with written informed consent from patients prior to undergoing surgery. In addition, the studies were conducted in strict accordance with the Declaration of Helsinki Principles.

Dermal skin sections were comminuted and digested in a 0.05% collagenase solution (Gibco) overnight at 37 °C. Following digestion, the suspension was centrifuged at 400 g for 10 min before removing the supernatant and re-suspending the resulting cell pellet prior to transfer into a tissue flask. Fibroblasts were incubated in Dulbecco's Modified Eagle's Medium (DMEM, Invitrogen, high glucose) supplemented with fetal calf serum (10%, FCS, Hyclone), penicillin, streptomycin and L-glutamine (all Invitrogen). Fibroblasts were maintained in a humidified atmosphere (5% CO_2) at 37 °C with the medium refreshed every 3 – 5 days. All cells used were at P5.

2.4. Cell Seeding onto Scaffolds

Prior to cell seeding, 8 mm diameter circular scaffolds were prepared from the square scaffolds using a biopsy punch (Stiefel). Each scaffold was sterilized under UV irradiation for 20 min on each side and placed in a graded ethanol series (100%, 90%, 70%) to pre-wet the scaffolds [50], followed by washing three times in phosphate buffered saline (PBS) before overnight incubation in medium (DMEM). Human dermal fibroblasts were seeded using a top seeding static method onto each scaffold (2×10^4 cells / scaffold). Fibroblasts were seeded and maintained in DEME (10% FCS)

supplemented with 50 μg/mL ascorbic acid (Sigma Aldrich) for either 7 or 14 days, with media replaced every alternate day. On completion, the scaffolds were fixed as described below and prepared for analysis; all scaffolds were visualized with immunofluorescence and SEM, while fibroblast infiltration was additionally assessed with histology.

2.5. Immunofluorescence

Cell-scaffold constructs were removed from the media, washed three times in PBS (containing Mg^{2+} and Ca^{2+}) and fixed in 4% paraformaldehyde at 4 °C for 12 h. Constructs were removed from the fixative and the cells permeabilized in 0.2% Tween 20 for 75 min at room temperature (RT), and incubated in 1% bovine serum albumin for 1 h at 37 °C to block nonspecific binding. Between each step, the scaffolds were washed three times with PBS. Scaffolds were then probed for nuclei (propidium iodide, Sigma, 1 μg/mL) and f-actin, (Alexa Fluor 488 phalloidin, Invitrogen, 200U/mL) by incubation in phalloidin for 20 min at RT, washed three times in PBS, followed by incubation in propidium iodide for a further 20 min at RT. Fluorescence images were captured using a Leica TCS SP5 confocal laser scanning microscope (Leica Microsystems, Wetzlar, Germany) at λ_{Ex} 495 and λ_{Em} 535 for visualization of f-actin, λ_{Ex}518 and λ_{Em} 617 for nuclei, and λ_{458} in reflectance mode for visualization of the scaffold fibers. Images were collected along the z-axis of the scaffold at 1.5 μm intervals then merged together to give a projected 3D representation.

2.6. Scanning Electron Microscopy

Cell-scaffold constructs were fixed in 3% glutaraldehyde in 0.1 M cacodylate buffer at 4 °C for a minimum of 12 h prior to SEM analysis. After fixation the constructs were placed into 0.1 M cacodylate buffer (2 × 10 min), osmium tetroxide (1 h) and ddH_2O (2 × 10 min) before dehydration in graded ethanol series (50% 2 × 10 min, 70% 2 × 10 min, 90% 2 × 10 min, 100% 2 × 15 min) and final immersion in hexamethyldisilazane (2 × 30 min). Constructs were allowed to dry for 2 h, then mounted onto stubs, and left overnight to ensure complete removal of solvent. Constructs and blank

scaffolds were gold sputter-coated for SEM visualization (FEI Quanta 200 Environmental SEM) using an accelerating voltage of 10 kV.

2.7. Histology and Immunohistochemistry

Cell-scaffold constructs were fixed in 4% PFA at 4 °C for a minimum of 12 h. To facilitate infiltration of the OCT embedding media (Tissue-Tek) and reduce possible ice crystal formation, the constructs were placed in a series of solutions (20% sucrose, 40% sucrose, 40% sucrose/20% OCT, 20% sucrose/60% OCT; in PBS, 2 h each) before finally being placed in 100% OCT (2 h) and frozen in liquid nitrogen. Samples were sectioned using a cryostat (Leica) at -20 °C, with 5 μm sections collected on Superfrost Plus® (HD Scientific) microscope slides. Following sectioning, the cell-scaffold constructs were stained using hematoxylin and eosin (both HDS Scientific). Briefly, sections were washed in PBS followed by staining with Harris' hematoxylin for 10 min, and eosin for 5 min. Samples were then dehydrated, and mounted with cover slips using PERTEX mounting medium. Sections of the cell-scaffold constructs were stained for the production of dermal ECM proteins collagen type I and fibronectin. Following cryosectioning, sections were washed in PBS, and non-specific binding was blocked using 1% BSA in PBS/0.1% Tween 20. Primary antibodies were diluted in 1% BSA/PBST and incubated on the sections for 2 h at RT. Primary antibodies used were monoclonal mouse anti-human collagen type I (MP Biomedicals, 1:1000) and monoclonal mouse anti-human fibronectin (BD Biosciences, 1:500). Antibody detection was performed using the Mach4 Universal HRP polymer detection kit (Biocare Medical). Following incubation with the primary antibodies, sections were incubated with horseradish peroxidase (HRP)-conjugated anti-mouse secondary antibodies for 15 min at RT (Biocare Medical). HRP was detected using 3,3'-diaminobenzidine tetrahydrochloride (DAB, Biocare Medical) through formation of brown pigmentation. Sections were then counterstained with hematoxylin, dehydrated, and mounted with coverslips using PERTEX.

3. Results and Discussion

3.1. Scaffold Characterization

Melt electrospun scaffolds were prepared using two different methods. One was to prepared scaffolds containing randomly deposited fibers with the use of a static collector, while the other method used a collector attached to a movable x-y stage for melt electrospinning in a direct writing mode. An illustration of the x-y stage and melt electrospinning apparatus are shown in figure 1, as well as with the interlaced diagonal line program for movement of the stage. The simple method of moving the collector results in scaffolds with straight fibers and periodic placement when compared with scaffolds prepared onto a static collector as indicated by the SEM images in figure 2(a) and 2(b), respectively. Video footage capturing scaffold fabrication in a direct writing mode is shown in the supplementary data [S1]. Based on the parameters utilized for fabrication of the reported scaffolds, manufacture time per scaffold was approximately 120 mins, though alteration to scaffold parameters, particularly diameter and pore size can decrease the time of fabrication. The straight fiber morphology is dependent on the translational speed of the collector, whereby straight fibers can be obtained if the collector is translated at a faster speed than the depositing viscous jet [37]. In this case, the translational speed of 2.5×10^{-2} m/s resulted in the fiber morphology seen in figure 2(a). Irrespective of the mode of collection, the fibers were smooth and defect-free and exhibited good interconnectivity between pores. Evidence of fiber fusion in the direct written scaffolds is shown in figure 2(a) insert. While fusion did not occur at all fiber junctions, similar results have previously been shown at a comparable collection distance [35], as degree of fiber fusion is due to the rate at which the molten polymer jet cools prior to collection.

Fiber diameter and pore size, (interfiber distance), were determined from SEM and optical microscope imaging, followed by analysis using Image J software. For both static and written scaffolds the fiber diameters were similar, namely, 6.8 ± 0.6 μm (average ± SD) for the static method and 7.5 ± 1.6 μm for the written approach ($p = 0.05$). In contrast, the pores were 16 ± 6 μm in size for the scaffolds prepared on the static collector compared with 46 ± 22 μm for the written scaffolds ($p =$

0.00). The distribution of fiber diameters and pore sizes for the electrospun scaffolds are shown in figure 3. When electrospinning onto a static collector, increasing the fiber diameter leads to a corresponding increase in pore size due to the interdependent relationship between these two parameters [51]. By accurately placing the fibers, with the aid of direct writing, the porosity of the electrospun mesh was further increased without increasing the fiber diameter.

In addition to SEM analysis, optical imaging of a representative scaffold (figure 4a) shows the long-range order obtainable using direct writing. The scaffolds could be readily handled without folding or breaking, although pressure from forceps can deform the scaffold (top of scaffold, figure 4(a)). Furthermore, the scaffolds could be analyzed via CT methods and Figure 4(b) shows a μ-CT micrograph of a representative scaffold. Orderly stacking of the fibers was shown, with a morphology not dissimilar to μ-CT imaging of FDM scaffolds [52], except that the fiber dimensions reported here are an order of magnitude smaller (7.5 ± 1.6 μm compared to c.a. 100 μm for FDM). With continual improvements in imaging technology, CT resolutions of less than 1 μm are now obtainable, making CT a viable characterization technique for scaffolds fabricated by electrospinning with low micron diameter fibers. In addition to 3D visualization, μ-CT enabled the calculation of scaffold porosity at 87%, which is similar compared to electrospun scaffolds previously reported [19]. Traditionally the porosity of electrospun scaffolds has been determined through mercury porosimetry or gravimetrical methods [53], however these have limitations as calculations are based on applied assumptions [54] while the pressure applied during porosimetry measurements can cause samples to collapse[52]. A movie capturing 3D visualization of the direct written scaffolds through μ-CT analysis is shown in the supplementary data [S2].

3.2. Evaluation of Dermal Fibroblast Infiltration

Seeding of dermal fibroblasts onto the PCL scaffolds was accomplished using a simple static top seeding method to examine the interactions and infiltration of the cells into the scaffolds. After 7 and 14 days *in vitro* the constructs were characterized with confocal microscopy, SEM and histology. Fibroblasts grown on 2D glass cover slips (figure 5(a)) and the electrospun written scaffold after 7

days *in vitro* (figure 5(b)) displayed typical elongated morphology; this was more pronounced when the fibroblasts were grown on the electrospun written scaffold. After 7 days *in vitro*, fibroblasts spanned across both the pores and fibers of the scaffold, as indicated in figure 5(b) by the yellow and white arrowheads, respectively. Previous studies using FDM scaffolds have shown that initial cellular attachment occurs at points of intersecting fibers [3, 55, 56], from where the attached cells migrate outwards. This is also reflected in this study (figure 5(b)), where an increase in fibroblast density is seen in regions with a greater proportion of intersecting fibers (red circle), compared to regions with a lower proportion of intersecting fibers (blue circle). After 14 days *in vitro*, the scaffold surface was completely covered by fibroblasts (figure 5(c)). Fibroblasts also bridged between adjacent scaffold struts, with inter-fiber distances ranging from 8 to 133 μm. Studies carried out by Sun *et al.* [57] have previously shown dermal fibroblasts are able to bridge distances up to 200 μm following 14 days *in vitro*. Fibroblast attachment to the scaffold shown in figure 5(b) highlights the scaffold dimensions achieved, concerning fiber diameter and pore size, are on a scale that is in relation to the size of the fibroblasts. The obtained fiber diameters and pore sizes have allowed the fibroblasts seeded on the scaffolds to 'view' and interact with them as a true 3D construct rather than a flat substrate.

The top, underside and cross-sections of the cell-scaffold constructs were evaluated for fibroblast infiltration using SEM. After 7 days *in vitro*, dermal fibroblasts had covered substantial areas of both the top and underside of the scaffold (figure 6(a)-(b)), while the cross-section (figure 6(c)) shows ECM deposited through the entire thickness of the scaffold. Figure 6(d), clearly shows cellular anchorage to the fibers, indicated by the arrows, and fibroblasts spanning across scaffold pores both laterally and through the scaffold thickness (z-axis). Figures 6(c) and 7(c) compare cross-sections of the constructs following 7 and 14 days *in vitro*, respectively, where an increase in the amount of ECM deposited between the two time points was evident. This confirms the infiltration of dermal fibroblasts throughout the entire thickness of the scaffold, and suggests cellular proliferation with increased incubation period. Figure 7(a), shows an SEM image of a continuous cell layer on the upper surface of the construct after 14 days, supporting immunofluorescence results (figure 5(c)).

The scaffolds reported within this study were fabricated by melt electrospinning, though, the attraction of solution electrospun scaffolds for TE applications stems from the ability to produce

nanofibers that hypothetically mimic the structural component of ECM [58]. However, nanofibers may not be as advantageous as microfibers for cell attachment, as previous studies have shown enhanced cellular proliferation on micron sized fibers compared to nanofibers [29, 59-62]. Interestingly, Chen *et al.* [61] found that for nanofibers, as fiber diameter increased, cellular adhesion and proliferation decreased but remained constant when fiber diameter was altered within the micron range. Furthermore, micron-scaled structures are an important element in bimodal scaffolds, where nanofibrous elements are combined with larger ones [30].

Fibroblast infiltration, in addition to SEM analysis, was assessed via histological methods on the cell-scaffold constructs after 14 days *in vitro*. A cross-section of the constructs stained with hematoxylin and eosin (H&E) shown in figure 8(a) revealed the presence and infiltration of cells throughout the scaffold. The expansion in figure 8(b) shows presence of fibroblast nuclei through the entire thickness of the scaffold, indicated by the black arrows. Round polymer fiber cross-sections (indicated by the yellow arrows) were evident throughout the scaffold and were coated with increased amount of cellular components due to the cells using the struts as their initial attachment points. In the continual pursuit to create scaffolds for TE applications, a key issue for consideration is the ability to obtain homogenous cellular colonization required to ultimately cultivate reconstructed tissue [27], a result which has been shown in the presented data.

A future goal for these PCL scaffolds is their use as a dermal component in the development of an *in vitro* skin model. In the quest to tissue engineer a dermal substitute, in addition to cellular infiltration of the scaffold material, production and deposition of ECM is a crucial requirement. While dermal ECM is comprised of many constituents, the main structural ECM molecule is collagen, with type I the most abundant within the dermis and as well as fibronectin, a key dermal ECM molecule. Immunohistochemical staining of the cell-scaffold constructs after 14 days *in vitro* for collagen type I and fibronectin shown in figures 8(c) and 8(d) respectively, confirm the presence of both these dermal ECM proteins. Both were distributed throughout the thickness of the scaffold, with the greatest density seen of collagen seen underneath the cells in the upper part of the construct. Negative controls for both collagen and fibronectin, replacing primary antibody incubation with the blocking solution did not show presence of the brown DAB precipitate (data not presented).

For an *in vitro* model to successfully mimic the functions of native skin, the formation of a basement membrane is crucial [63-65]. *In vitro* skin models currently detailed within the literature commonly use collagen gels [66, 67] or alternatively de-epidermised dermis as the dermal component [68], which retains the native basement membrane. When collagen gels have been used, the gels are seeded and conditioned with fibroblasts, onto which keratinocytes are seeded. This approach has been shown to achieve adequate separation between the dermal and epidermal layers, resulting in creation of the basement membrane *in vitro*. Formation of the fibroblast sheet on the seeded surface of the scaffold in the present study, in conjunction with the presence of collagen type I and fibronectin, displays the initial step of dermal layer formation, and a surface for subsequent seeding of keratinocytes. It is noteworthy that no evidence of scaffold contraction was observed after seeding the melt electrospun materials with fibroblasts, which may give them an advantage over substrates for which contraction can be a problem.

The ability to combine melt electrospinning and direct writing allows the fabrication of scaffolds with control over fiber diameter through manipulation of electrospinning variables [37], as well as control over fiber placement and therefore scaffold design. These factors increase the number of potential TE applications for scaffolds fabricated using this combination. The ability to produce aligned fibers as a way of directing cell growth has shown to be successful in the engineering of blood vessels [69] as well as in peripheral nerve regeneration [70]. Additionally, such an approach can be used in the design and fabrication of tubular scaffolds, whereby design parameters such as fiber diameter, the number of fibers and the fiber winding angle can be used to control scaffold features such as pore size and porosity [38].

Fibroblast attachment and infiltration throughout the thickness of the scaffolds indicates that direct written scaffolds are true 3D structures. TE scaffolds are often prepared by techniques such as particle leaching, thermal induced phase separation, electrospinning or various solid freeform (SFF) fabrication techniques [6_ENREF_6], with the fabrication method dependent on the desired end application. At one end of the spectrum, are nano-scale scaffolds, solution electrospun mats, could be regarded as a textured 2D substrate. As the resulting pore sizes of these scaffolds restrict cell infiltration, cell migration occurs across the surface rather than by infiltration into the scaffold. At the

other end of the spectrum are micron-scale SFF scaffolds, for which it could be similarly suggested that cells 'see' these scaffolds as curved 2D surfaces since these scaffold struts are, in general, an order of magnitude in size larger than the cells themselves. The results reported here show that fabrication of a scaffold that fills the void between the current nano- and micron- scale scaffolds allows fibroblasts to attach to and infiltrate though the electrospun written scaffolds, both in a lateral and vertical direction, producing a true 3D fibroblast-scaffold construct. This result is due to the fiber diameter and interfiber distance arrangement that can be produced through combining melt electrospinning with direct writing.

4. Conclusion

The current study uses melt electrospinning in combination with direct writing for the preparation of PCL scaffolds with micrometer sized fibers (7.5 ± 1.5 μm diameter) and interfiber distances suitable to allow cellular infiltration (46 ± 22 μm). Melt electrospun PCL fibers were collected a programmable x-y stage, resulted in the fibers being linearly placed, confirmed by both electron microscopy and micro-computed tomography. The electrospun written scaffolds were subsequently seeded and incubated with dermal fibroblasts, and cellular infiltration as well as ECM production was assessed through immunofluorescent, electron microscopy, histological and immunohistochemical evaluation. These results showed fibroblast infiltration throughout the scaffold, with H&E staining of the cell-scaffold constructs confirming fibroblast nuclei present, along with the production of key dermal ECM proteins, collagen type I and fibronectin, though the entire thickness of the scaffold.

While the PCL scaffolds shown here are currently being investigated for TE of skin, demonstration of a true 3D cell-scaffold construct developed through the electrospinning writing of polymers, and more importantly control over scaffold design, paves the way for precision-made scaffolds. The real utility of melt electrospinning in a direct writing mode is that it produces porous scaffolds on a scale that fills the current research gap between solution electrospinning and many of the conventional AM techniques.

Acknowledgements

The authors are grateful to the expertise of Dr. Christina Theodoropoulos (Analytical Electron Microscopy Facility, Queensland University of Technology) for assistance with SEM preparation. Mr. Dennis Dwarte (Australian Centre for Microscopy & Microanalysis, Sydney University) for μ-CT data collection, Michael Plum for help with illustrations, and Dr Ferry Melchels (QUT) who assisted with μ-CT data analysis and interpretation. Dr Leonore de Boer (Cell Imaging Facility, Queensland University of Technology) was also helpful with confocal imaging. We also acknowledge Dr Anthony Kane and his staff, plus the patients for their generous donations of time and skin samples, and Ms. Rebecca Dawson, for collection of the donated skin samples. The funding for this project was provided by the Wound Management Innovation Cooperative Research Centre (WMICRC).

References

1. Hutmacher D, Woodfield T, Dalton P and Lewis J. Scaffold design and fabrication. In: Blitterswijk Cv, Thomsen P, Lindahl A, Jeffrey H, Williams DF, Cancedda R, et al., editors. Tissue Engineering. Burlington: Academic Press; 2008. p. 403-54.
2. Lewis J A 2006 *Adv. Funct. Mater.* **16** 2193-204
3. Hutmacher D W, Schantz T, Zein I, Ng K W, Teoh S H and Tan K C 2001 *J. Biomed. Mater. Res.* **55** 203-16
4. Hutmacher D W and Cool S 2007 *J. Cell. Mol. Med.* **11** 654-69
5. Goodridge R D, Tuck C J and Hague R J M 2012 *Prog. Mater. Sci.* **57** 229-67
6. Dalton P D, Woodfield T and Hutmacher D W 2009 *Biomaterials* **30** 701-2
7. Smay J E, Cesarano J and Lewis J A 2002 *Langmuir* **18** 5429-37
8. Smay J E, Gratson G M, Shepherd R F, Cesarano J and Lewis J A 2002 *Adv. Mater.* **14** 1279-83
9. Teo W E and Ramakrishna S 2006 *Nanotechnology* **17** R89-R106
10. Pham Q P, Sharma U and Mikos A G 2006 *Tissue Eng.* **12** 1197-211
11. Subbiah T, Bhat G S, Tock R W, Parameswaran S and Ramkumar S S 2005 *J. Appl. Polym. Sci.* **96** 557-69
12. Li M, Mondrinos M J, Chen X, Gandhi M R, Ko F K and Lelkes P I 2006 *J. Biomed. Mater. Res. A* **79A** 963-73
13. Gerardo-Nava J, Führmann T, Klinkhammer K, Seiler N, Mey J, Klee D, Möller M, Dalton P D and Brook G A 2009 *Nanomedicine* **4** 11-30
14. Ekaputra A K, Prestwich G D, Cool S M and Hutmacher D W 2008 *Biomacromolecules* **9** 2097-103
15. Yang F, Murugan R, Wang S and Ramakrishna S 2005 *Biomaterials* **26** 2603-10
16. Wan L-S and Xu Z-K 2009 *J. Biomed. Mater. Res. A* **89A** 168-75
17. Zhang Y, Ouyang H, Lim C T, Ramakrishna S and Huang Z-M 2005 *J. Biomed. Mater. Res. B* **72B** 156-65
18. Sisson K, Zhang C, Farach-Carson M C, Chase D B and Rabolt J F 2010 *J. Biomed. Mater. Res. A* **94A** 1312-20
19. Cipitria A, Skelton A, Dargaville T R, Dalton P D and Hutmacher D W 2011 *J. Mater. Chem.* **21** 9419-53
20. Cui W, Chang J and Dalton P D. Electrospun Fibers for Drug Delivery. In: Ducheyne P, Healy K, Hutmacher DW, Grainger DW, Kirkpatrick CJ, editors. Comprehensive Biomaterials: Elsevier; 2011. p. 445-62.
21. Schneider O D, Loher S, Brunner T J, Uebersax L, Simonet M, Grass R N, Merkle H P and Stark W J 2008 *J. Biomed. Mater. Res. B* **84B** 350-62
22. Simonet M, Schneider O D, Neuenschwander P and Stark W J 2007 *Polym. Eng. Sci.* **47** 2020-6
23. Nam J, Huang Y, Agarwal S and Lannutti J 2007 *Tissue Eng.* **13** 2249-57
24. Tzezana R, Zussman E and Levenberg S 2008 *Tissue Eng. Part C Methods* **14** 281-8
25. Zhang D and Chang J 2008 *Nano. Lett.* **8** 3283-7
26. Uttayarat P, Perets A, Li M, Pimton P, Stachelek S J, Alferiev I, Composto R J, Levy R J and Lelkes P I 2010 *Acta Biomater.* **6** 4229-37
27. Vaquette C and Cooper-White J J 2011 *Acta Biomater.* **7** 2544-57
28. Blakeney B A, Tambralli A, Anderson J M, Andukuri A, Lim D-J, Dean D R and Jun H-W 2011 *Biomaterials* **32** 1583-90
29. Soliman S, et al. 2010 *Acta Biomater.* **6** 1227-37
30. Kim S J, Jang D H, Park W H and Min B-M 2010 *Polymer* **51** 1320-7

31. Centola M, Rainer A, Spadaccio C, Porcellinis S D, Genovese J A and Trombetta M 2010 *Biofabrication* **2** 014102
32. Ahn S, Koh Y H and Kim G 2010 *J. Micromech. Microgen.* **20** 065015
33. Hosseinkhani H, Hosseinkhani M, Hattori S, Matsuoka R and Kawaguchi N 2010 *J. Biomed. Mater. Res. A* **94A** 1-8
34. Hutmacher D W and Dalton P D 2011 *Chem. - Asian J* **6** 44-56
35. Dalton P D, Joergensen N T, Groll J and Moeller M 2008 *Biomed. Mater.* **3** 034109
36. Dalton P D, Grafahrend D, Klinkhammer K, Klee D and Möller M 2007 *Polymer* **48** 6823-33
37. Brown T D, Dalton P D and Hutmacher D W 2011 *Adv. Mater.* **23** 5651-7
38. Brown T, Slotosch A, Thibaudeau L, Taubenberger A, Loessner D, Vaquette C, Dalton P and Hutmacher D 2012 *Biointerphases* **7** 1-16
39. Asselineau D and Prunieras M 1984 *Br. J. Dermatol.* **111** 219-21
40. Bell E, et al. 1983 *J. Investig. Dermatol.* **81** 2s-10s
41. Bell E, Ehrlich H P, Buttle D J and Nakatsuji T 1981 *Science* **211** 1052-4
42. Bell E, Ivarsson B and Merrill C 1979 *Proc. Nat. Acad. Sci.USA* **76** 1274-8
43. Blackwood K A, et al. 2008 *Biomaterials* **29** 3091-104
44. Powell H M and Boyce S T 2009 *Tissue Eng.* **15** 2177-87
45. Chong E J, Phan T T, Lim I J, Zhang Y Z, Bay B H, Ramakrishna S and Lim C T 2007 *Acta Biomater.* **3** 321-30
46. Cooper M L, Hansbrough J F, Spielvogel R L, Cohen R, Bartel R L and Naughton G 1991 *Biomaterials* **12** 243-8
47. Ng K W, Khor H L and Hutmacher D W 2004 *Biomaterials* **25** 2807-18
48. Detta N, Brown T D, Edin F K, Albrecht K, Chiellini F, Chiellini E, Dalton P D and Hutmacher D W 2010 *Polym. Int.* **59** 1558-62
49. Melchels F P W, Barradas A M C, van Blitterswijk C A, de Boer J, Feijen J and Grijpma D W 2010 *Acta Biomater.* **6** 4208-17
50. Mikos A G, Lyman M D, Freed L E and Langer R 1994 *Biomaterials* **15** 55-8
51. Eichhorn S J and Sampson W W 2005 *J. R. Soc. Interface.* **2** 309-18
52. Ho S T and Hutmacher D W 2006 *Biomaterials* **27** 1362-76
53. Nisbet D R, Rodda A E, Finkelstein D I, Horne M K, Forsythe J S and Shen W 2009 *Colloids Surf. B: Biointerfaces* **71** 1-12
54. Webb P A and Orr C. Analytical Methods in Fine Particle Technology: Micromeritics Instrument Corp; 1997.
55. Sun T, Smallwood R and MacNeil S 2009 *J. Mater. Sci. Mater. Med.* **20** 1483-93
56. Engelmayr J G C, Papworth G D, Watkins S C, Mayer J J E and Sacks M S 2006 *J. Biomech.* **39** 1819-31
57. Sun T, Norton D, McKean R J, Haycock J W, Ryan A J and MacNeil S 2007 *Biotechnol. Bioeng.* **97** 1318-28
58. Li W-J, Laurencin C T, Caterson E J, Tuan R S and Ko F K 2002 *J. Biomed. Mater. Res.* **60** 613-21
59. Pham Q P, Sharma U and Mikos A G 2006 *Biomacromolecules* **7** 2796-805
60. Badami A S, Kreke M R, Thompson M S, Riffle J S and Goldstein A S 2006 *Biomaterials* **27** 596-606
61. Chen M, Patra P K, Warner S B and Bhowmick S 2007 *Tissue Eng.* **13** 579-87
62. Guex A G, Kocher F M, Fortunato G, Körner E, Hegemann D, Carrel T P, Tevaearai H T and Giraud M N 2012 *Acta Biomater.* **8** 1481-9
63. Stark H-J, Willhauck M J, Mirancea N, Boehnke K, Nord I, Breitkreutz D, Pavesio A, Boukamp P and Fusenig N E 2004 *Eur. J. Cell Biol.* **83** 631-45

64. Boehnke K, Mirancea N, Pavesio A, Fusenig N E, Boukamp P and Stark H-J 2007 *Eur. J. Cell Biol.* **86** 731-46
65. Smola H, Stark H-J, Thiekötter G, Mirancea N, Krieg T and Fusenig N E 1998 *Exp. Cell Res.* **239** 399-410
66. Marionnet C, Pierrard C, Vioux-Chagnoleau C, Sok J, Asselineau D and Bernerd F 2006 *J. Invest. Dermatol.* **126** 971-9
67. Marionnet C, Vioux-Chagnoleau C, Pierrard C, Sok J, Asselineau D and Bernerd F 2006 *Exp. Dermatol.* **15** 625-33
68. Xie Y, Rizzi S C, Dawson R, Lynam E, Richards S, Leavesley D I and Upton Z 2010 *Tissue Eng. Part C Methods* **16** 1111-23
69. Xu C Y, Inai R, Kotaki M and Ramakrishna S 2004 *Biomaterials* **25** 877-86
70. Schnell E, Klinkhammer K, Balzer S, Brook G, Klee D, Dalton P and Mey J 2007 *Biomaterials* **28** 3012-25

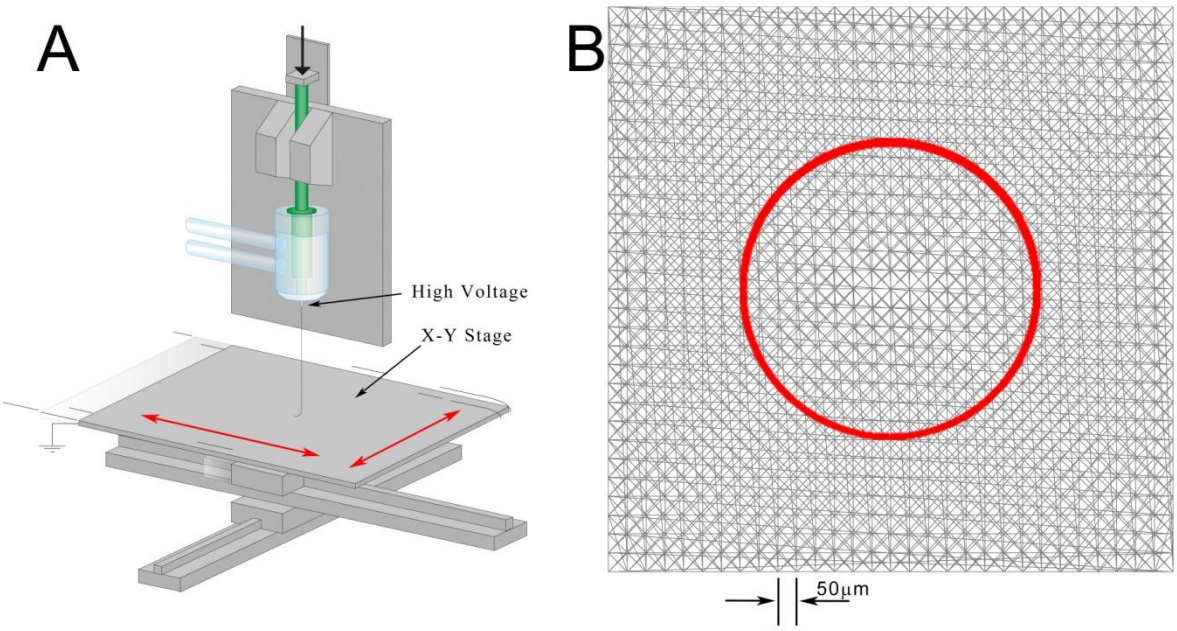

Figure 1: A) A schematic of the apparatus used to produce the melt electrospun scaffolds in a direct writing mode. B) The pattern used to program the x-y stage and produce the electrospun written scaffolds. The pattern length and height was 15 mm, and the red ring indicates approximately where scaffolds were cut with a biopsy punch. (Note: pattern is not drawn to scale)

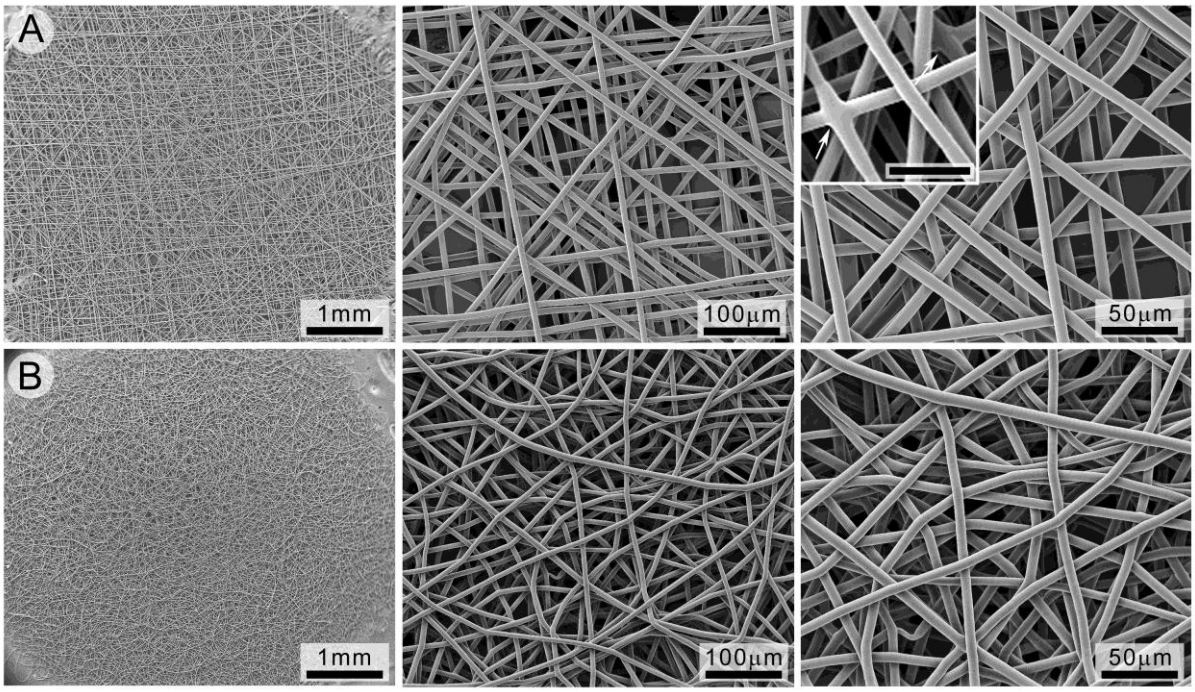

Figure 2: Scanning electron microscopy of PCL scaffolds comparing fiber morphology and orientation for melt electrospun scaffolds via A) direct writing, evidence of fused fibers indicated by the arrows in the insert (scale bar = 50 μm) and B) static conditions.

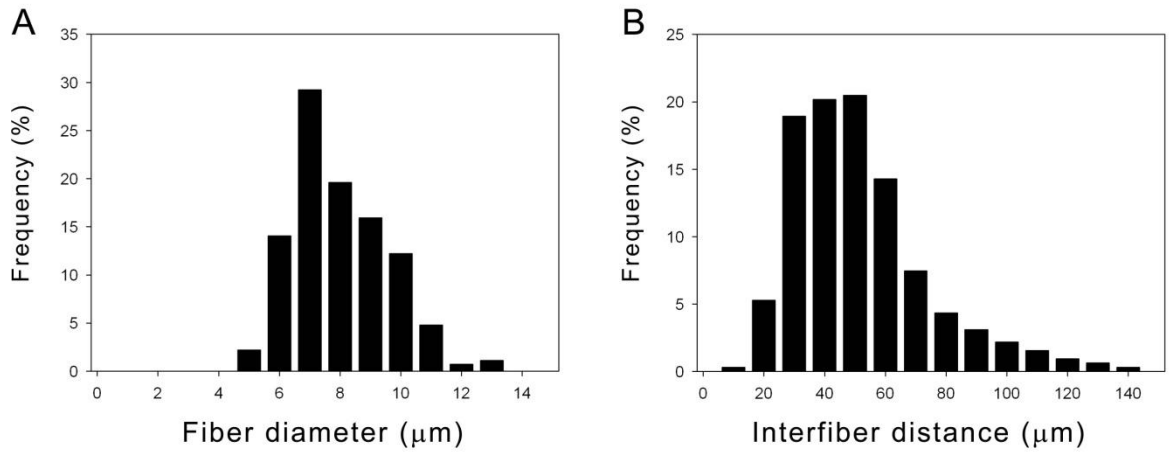

Figure 3: Frequency histograms for electrospun written scaffolds showing A) fiber diameters ranging from 4.1 μm to 12.8 μm with an average diameter ± SD of 7.5 ± 1.6 μm, and B) the inter-fiber distance ranging from 8 μm to 133 μm, with an average of 46 ± 22 μm. (n=30).

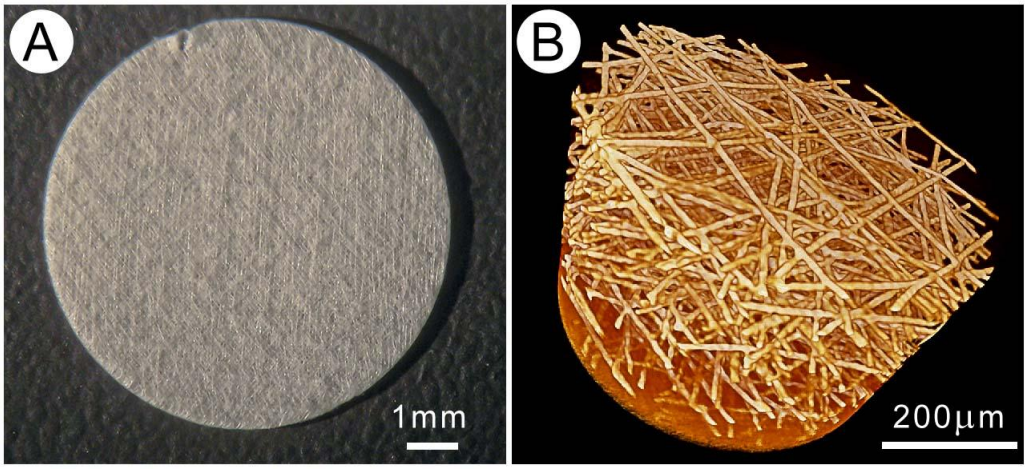

Figure 4: Visualization of a melt electrospun scaffold produced in a direct writing mode through A) optical and B) µ-CT methods.

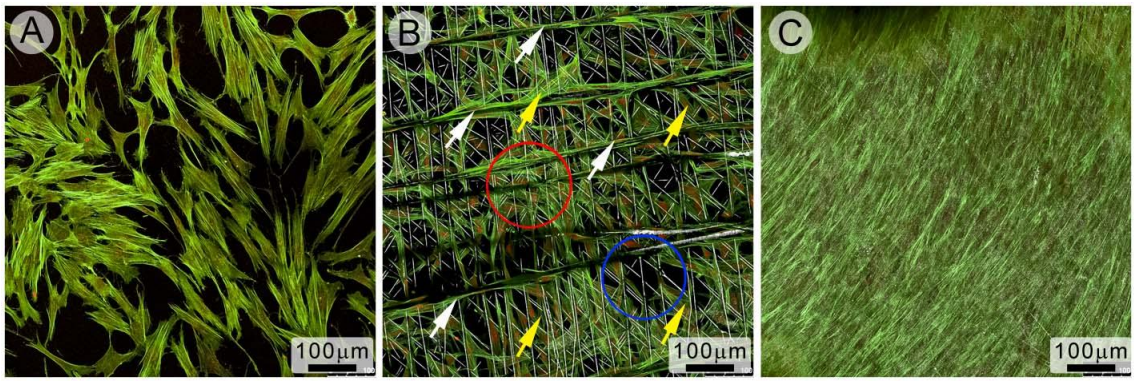

Figure 5: Scanning laser confocal microscopy of fibroblasts on A) a glass cover slip, and the electrospun written scaffolds following B) 7 and C) 14 days. The white arrows in B show fibroblast migration along the fibers and the yellow arrows show spreading across scaffold voids. Regions within the scaffold of high and low fiber intersections/density and corresponding high and low fibroblast density are shown by the red and blue circles, respectively. Cell-scaffold constructs were stained with phalloidin (green) and propidium iodide (red), for visualization of actin filaments and nuclei, respectively.

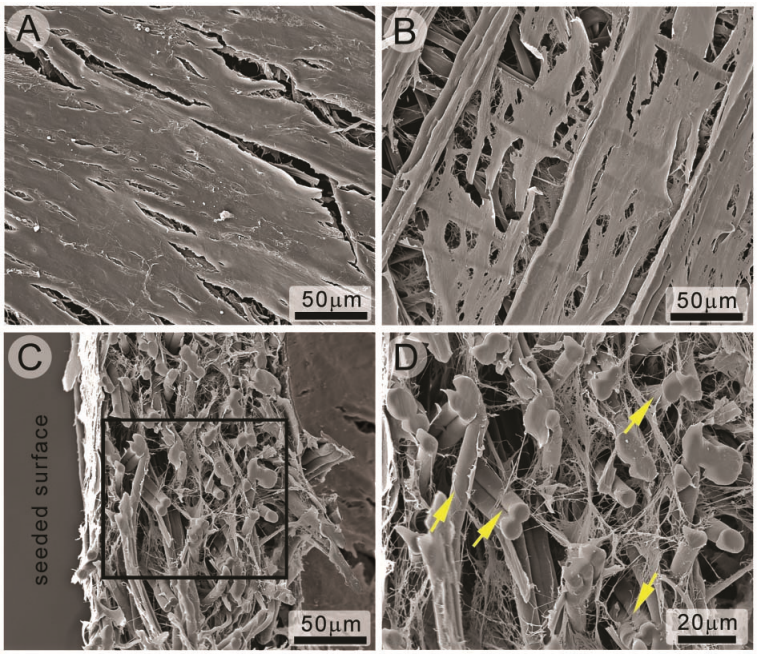

Figure 6: Fibroblast infiltration of the electrospun written scaffold after 7 days was assessed via SEM. Micrographs show fibroblasts present on the A) top side, B) underside, and C) within the thickness of the scaffold, with D) a magnified image of C. The arrows in D indicate points of fibroblast attachment and anchorage to the PCL fibers. The image shown in D represents the highlighted scaffold segment in C.

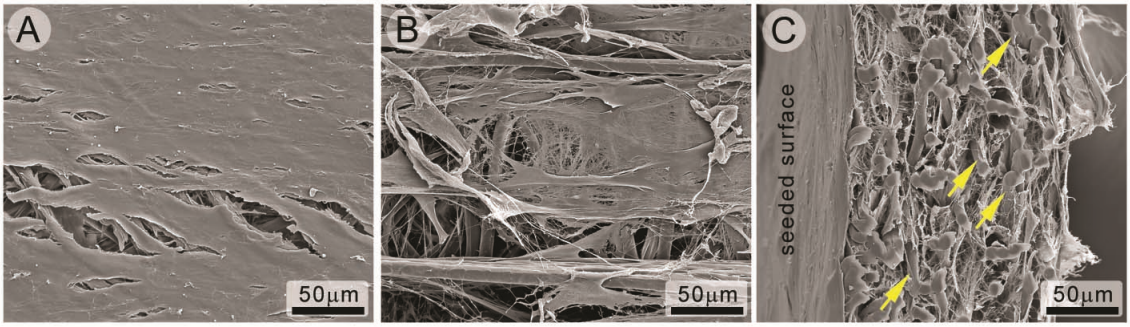

Figure 7: Fibroblast infiltration of the electrospun written scaffold after 14 days was assessed via SEM. Micrographs show fibroblasts present on the A) top side, B) underside, and C) within the thickness of the scaffold. The arrows in C indicate points of fibroblast attachment to the PCL fibers.

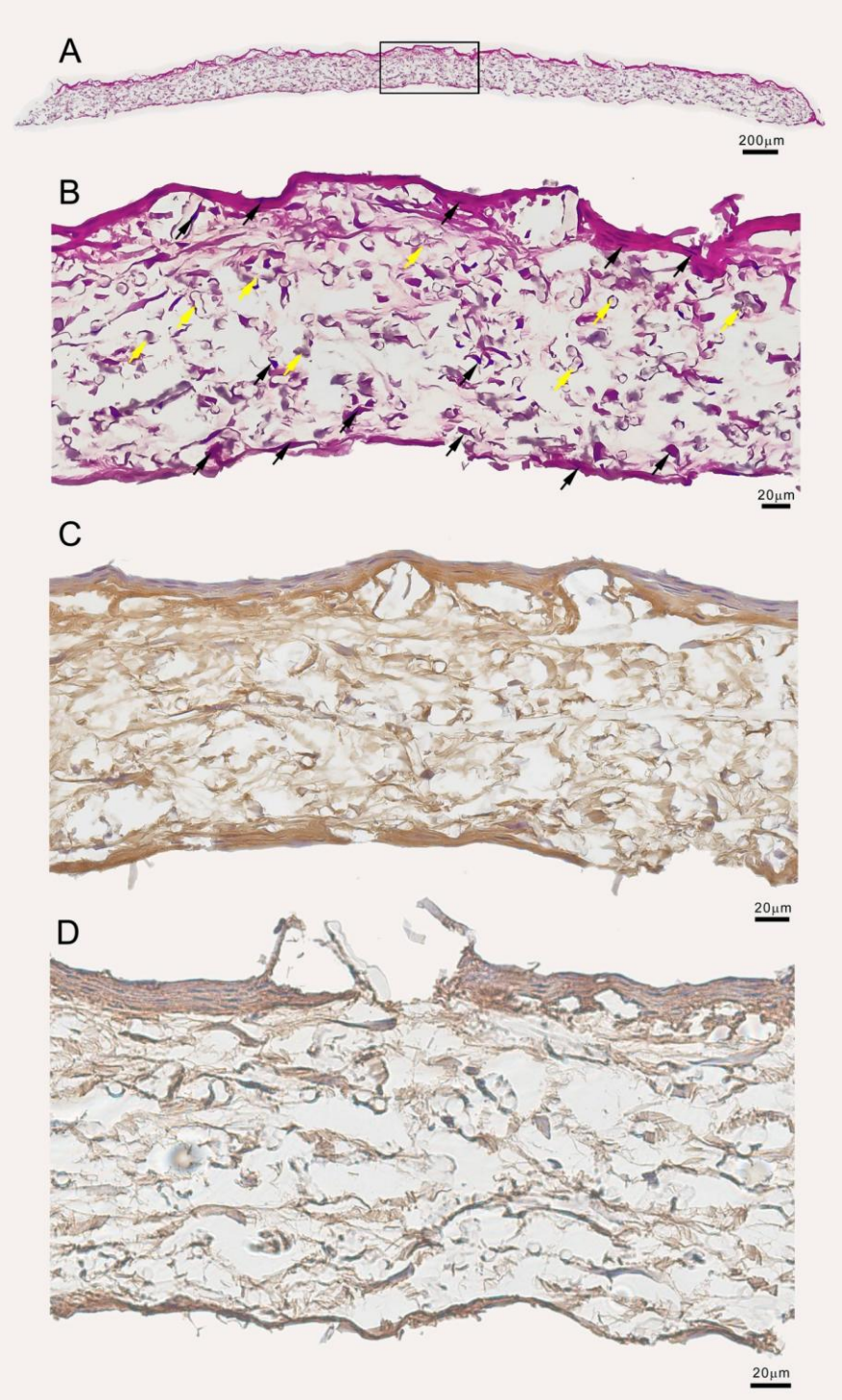

Figure 8: H&E and immunohistochemical staining of the cell-scaffold constructs after 14 days. H&E staining of A) the entire scaffold, and B) an expansion. Fibroblast nuclei were found through the entire thickness of the scaffold as indicated by the black arrows (B). The yellow arrows show PCL fibers within the stained section. Immunohistochemical staining for C) collagen type I, and D) fibronectin. Staining for collagen type I and fibronectin showed both ECM proteins were deposited by the fibroblasts throughout the thickness of the scaffold.